HIGH-TEMPERATURE STABILITY OF LAURITE AND Ru–Os–Ir ALLOY AND THEIR ROLE IN PGE FRACTIONATION IN MAFIC MAGMAS

JAMES M. BRENAN[§] AND DAVID ANDREWS

Department of Geology, University of Toronto, 22 Russell Street, Toronto, Ontario M5S 3B1, Canada

ABSTRACT

Experiments were performed to establish the stability limits and mineral – sulfide melt partitioning behavior of the platinum-group minerals laurite $(Ru,Os,Ir)S_2$ and Ru–Os–Ir alloy as functions of temperature and sulfur fugacity. Ruthenium-doped experiments yielded laurite up to ~1275 °C at log $f(S_2)$ of –2.0, with laurite replaced by Ru alloy at higher temperature. Similar results were observed at log $f(S_2)$ of –2 and –1.3 for compositions doped with multiple PGE, except that Ru–Os–Ir alloy coexisted with laurite at T ≤ 1265°C. Laurite and alloy from these latter experiments were found to be Ru–Os–Ir-rich and Pt–Pd-poor, with grains of alloy containing more Os and Ir than laurite, and both phases becoming (Os + Ir)-rich with increasing $f(S_2)$. Concentrations of PGE in sulfide liquid saturated with laurite ± alloy were found to be: Ru: 1–13 wt%; Os and Ir: ≤ 0.6 wt%; Pt and Pd: 0.5–4 wt%. The finding that laurite and Ru–Os–Ir alloy are stable at chromian-spinel-based liquidus temperatures indicates that the commonly observed inclusion of these phases in chromian spinel can be interpreted as a primary magmatic texture. High solubilities for Ru in molten sulfide, combined with low intrinsic abundances of the PGE in igneous rocks, suggest that crystallization of laurite or Ru–Os–Ir alloy in the presence of immiscible sulfide liquid is unlikely. Thus, the extent to which PGE-bearing accessory minerals will affect the final distribution of the PGE within an igneous body may be strongly linked to when, or if, saturation in sulfide liquid occurs.

Keywords: laurite, alloy, platinum-group minerals, platinum-group elements, partitioning, experiments.

SOMMAIRE

Nous décrivons les résultats d'expériences conçues dans le but d'établir les limites de la stabilité des phases minérales laurite [Ru,Os,Ir)S$_2$] et un alliage de Ru–Os–Ir, et la répartition d'éléments du groupe du platine (EGP) en présence de ces phases et d'un liquide sulfuré en fonction de la température et de la fugacité du soufre. Les expériences, qui ont porté sur des mélanges dopés au ruthénium, ont donné de la laurite jusqu'à environ 1275°C à une valeur de log $f(S_2)$ de –2.0; à plus haute température, la laurite est déstabilisée aux dépens de l'alliage à dominance de Ru. Les expériences portant sur des compositions dopées avec d'autres éléments du groupe du platine à une valeur de log $f(S_2)$ de –2 et –1.3 ont donné des résultats semblables, sauf que l'alliage Ru–Os–Ir coexiste avec la laurite à une température inférieure ou égale à 1265°C. La laurite et l'alliage dans ces derniers cas sont riches en Ru–Ir–Os et montrent de faibles teneurs en Pt et Pd, les grains d'alliage contenant plus d'osmium et d'iridium que la laurite, et les deux phases devenant progressivement plus riches en Os + Ir avec une augmentation en $f(S_2)$. Le liquide sulfuré saturé en laurite ± alliage contient 1–13% en poids de Ru, ≤0.6% de Os et Ir, et entre 0.5 et 4% de Pt et Pd. Le fait que la laurite et l'alliage Ru–Os–Ir soient stables à une température du liquidus, telle que calibrée au moyen du spinelle chromifère, montre que les exemples répandus de ces phases piégées dans le spinelle chromifère marqueraient une relation primaire et donc magmatique. A cause des solubilités élevées du Ru dans le liquide sulfuré, ainsi que des abondances limitées des EGP dans les roches ignées, la cristallisation de la laurite ou de l'alliage Ru–Os–Ir en présence d'un liquide sulfuré immiscible semble peu probable. Le rôle des minéraux accessoires porteurs des EGP dans la distribution finale de ceux-ci dans un complexe igné dépendrait donc fortement de la présence ou non d'un liquide sulfuré et du stade de son apparition.

(Traduit par la Rédaction)

Mots-clés: laurite, alliage, minéraux du groupe du platine, éléments du groupe du platine, répartition, expériences.

[§] *E-mail address*: brenan@geology.utoronto.ca

INTRODUCTION

Numerous studies have shown that the IPGE (the iridium subgroup of the platinum-group elements: Os, Ir, Ru) and the PPGE (the palladium subgroup of the platinum-group elements: Pt, Pd, Rh) behave very differently in mafic and ultramafic magmatic systems [see Crocket (1981) and Barnes *et al.* (1985) for summaries]. Whereas the IPGE generally show compatible geochemical behavior, the PPGE exhibit relative enrichment as a function of degree of differentiation. For example, primitive lavas whose compositions are dominantly controlled by fractionation of olivine (± chromian spinel) yield apparent partition coefficients (*D*) for the IPGE (especially Ir) that are 6 or more, whereas values for the PPGE are ~1 or less (Barnes & Picard 1993, Brügmann *et al.* 1987). These elements thus become decoupled in the more evolved members of such lava suites. In the case of plutonic rocks, examples of this decoupling include the strong enrichment in Os, Ir, and Ru relative to Pt, Pd and Rh in cumulate chromitite horizons in ophiolitic complexes worldwide (Barnes *et al.* 1985), upward increases in the ratio of Pt + Pd to Os + Ir + Ru in silicate and chromitite cumulate horizons from layered intrusions (*e.g.,* Bushveld; Maier & Barnes 1999), and IPGE enrichment in basal cumulates relative to values inferred for parental magmas (*e.g.,* the Heazlewood River Complex; Peck *et al.* 1992). In this paper, we present the results of phase equilibrium and partitioning experiments to support the notion that such IPGE–PPGE decoupling can arise by early precipitation of IPGE-bearing accessory minerals at the magmatic stage.

BACKGROUND INFORMATION

Various hypotheses have been put forth to account for the apparent decoupling of the PGE, including 1) compatibility of the IPGE in primary magmatic phases such as olivine and chromian spinel (Hart & Ravizza 1996, Brügmann *et al.* 1987, Barnes & Picard 1993, Capobianco & Drake 1990, Capobianco *et al.* 1994, Peach & Mathez 1996), 2) preferential partitioning of IPGE into monosulfide solid-solution, *Mss* (Li *et al.* 1998, Barnes *et al.* 1997, Fleet *et al.* 1993), or 3) early saturation of an IPGE-rich alloy or sulfide (Maier & Barnes 1999, Fleet & Stone 1991, Tredoux *et al.* 1995, Legendre & Augé 1986). Recent field-based observations (*e.g.,* Maier & Barnes 1999, Maier *et al.* 1999) have indicated that the IPGE are excluded from chromian spinel and olivine, thus suggesting that sulfide or alloy phases may be responsible for the observed IPGE–PPGE decoupling. The possible role of IPGE alloy or sulfide in this regard is highlighted by numerous detailed petrographic studies that have documented a variety of platinum-group minerals (PGM) as inclusions within chromian spinel from layered intrusions (*e.g.,* Talkington & Lipin 1986, Maier *et al.* 1999, and refer-

ences therein) and ophiolites (*e.g.,* Prichard *et al.* 1986, Torres-Ruiz *et al.* 1996, Nakagawa & Franco 1997, Garuti *et al.* 1999, and references therein). In their study of world-wide occurrences of ophiolite, Legendre & Augé (1986) identified thirteen different platinum-group minerals (PGM), of which laurite [(Ru,Os,Ir)S$_2$] and rutheniridosmine (Ru–Ir–Os alloy) were observed to be the most abundant included phases, whereas Pt, Pd and Rh-bearing PGM were found to be notably sparse. In this and other studies, textural observations indicate that laurite or Ru–Ir–Os-alloy (or both) coprecipitated with chromian spinel. Furthermore, petrographic studies by Peck *et al.* (1992) have identified chromian spinel, olivine and pyroxene *inclusions* within alluvial grains of Os–Ir–Ru alloy weathered from the Heazlewood River Complex (Tasmania). Thus, inclusion–host relations documented from these latter studies would suggest that IPGE-rich sulfide and alloy phases were precipitating at the same time as the primary igneous minerals during magma emplacement.

Simultaneous crystallization of an IPGE-rich sulfide or alloy along with primary magmatic silicate and oxide minerals, followed by fractionation and accumulation, could account for the observed decoupling of the IPGE and PPGE in the aforementioned examples. In addition to the textures revealed by natural samples, a first-order assessment of whether IPGE sulfides and alloys are likely to be near-liquidus phases requires information bearing on 1) the solubility of these minerals in mafic and ultramafic melt compositions, and 2) the relative stabilities of these minerals as functions of temperature and the fugacities of oxygen, $f(O_2)$, and sulfur, $f(S_2)$. Although the data are scarce to assess PGM solubilities, direct measurements involving pure metals (*e.g.,* O'Neill *et al.* 1995, Ertel *et al.* 1999, Amossé *et al.* 2000) generally reveal low solubilities at $f(O_2)$ relevant to the genesis of terrestrial magmas, althouth the results of Peach & Mathez (1996) suggest that Ir solubilities may be enhanced in the presence of dissolved sulfur. In either case, still lower values may be expected if metal activities are reduced by dilution to form multicomponent PGM. Thus, concentrations required for saturation may approach levels present in mafic or ultramafic rock compositions, although further experimental work clearly is required. Given the plausibility of PGM saturation, the question remains as to whether the most common PGM, such as laurite, are indeed stable at temperatures corresponding to the silicate melt liquidus, and whether the compositions of coexisting PGM, such as laurite and Ru–Os–Ir alloy, are consistent with high-temperature equilibrium phase-relations. Although there are thermodynamic data available to evaluate these relations, uncertainties in the activity–composition relations for ternary Ru–Os–Ir sulfides and alloys, combined with the relatively large uncertainties in heat capacity and enthalpy data for these minerals, make accurate determination of high-temperature phase relations difficult at best. In order to redress these shortcomings, we have

performed experiments to determine the stability limits of the IPGE-rich PGM laurite and Ru–Os–Ir alloy at controlled temperature, $f(O_2)$ and $f(S_2)$. In addition, our phase-equilibrium experiments included a suite of PGE in order to establish laurite – and alloy – sulfide melt partition coefficients, which in turn can be used to assess the ability of these minerals to fractionate the IPGE from the PPGE. Results of these experiments confirm the notion that laurite and Ru–Os–Ir alloy can be stable liquidus phases in a mafic magma and that each of these phases selectively exclude the PPGE, thus lending strong support for the role of PGM in decoupling the PGE in mafic igneous systems.

Overview of experiments

The objectives of this study are to determine the high-temperature stability of laurite and Ru–Os–Ir alloy and to establish the role of these phases as selective collectors of the IPGE. Because natural laurite and IPGE-rich alloy contain relatively high levels of all three IPGE, our experiments are specifically focused on ternary IPGE compositions (near-chondritic), which broadly mimic those found in natural assemblages. At values of $f(O_2)$ appropriate for basalt petrogenesis, the PGE oxides are unstable, and thus the primary phase-relations of interest involve the stability of the sulfide and alloy phases. The relevant equilibria that define the stabilities of these phases can be expressed by the three end-member reactions:

$$Ru_{alloy} + S_2 = RuS_{2sulfide} \qquad (1)$$

$$Os_{alloy} + S_2 = OsS_{2sulfide} \qquad (2)$$

$$Ir_{alloy} + S_2 = IrS_{2sulfide} \qquad (3)$$

On the basis of existing thermodynamic data (Barin 1995), we have calculated the maximum thermal stability of the end-member sulfides in the binary system RuS_2–OsS_2 as a function of composition and the sulfur fugacities employed in our experiments. Results are portrayed in Figure 1. In this case, we have assumed ideal mixing in the sulfide and alloy phases, which is probably unrealistic, but serves for the purposes of illustration and as a guide to plan experiments. We have not calculated phase diagrams for the RuS_2–IrS_2 or OsS_2–IrS_2 binary systems owing to the known solvus that exists in the Ir-rich portion of these systems. Calculations bearing on the T–$f(S_2)$ stability of IrS_2 indicate, however, that IrS_2 and OsS_2 behave similarly. The calculated phase-diagram portrayed in Figure 1 predicts the relative variation in sulfide *versus* alloy stability as functions of $f(S_2)$ and composition. As depicted, reduction in $f(S_2)$ has a significant effect on decreasing the thermal stability of the sulfide phase, as does the addition
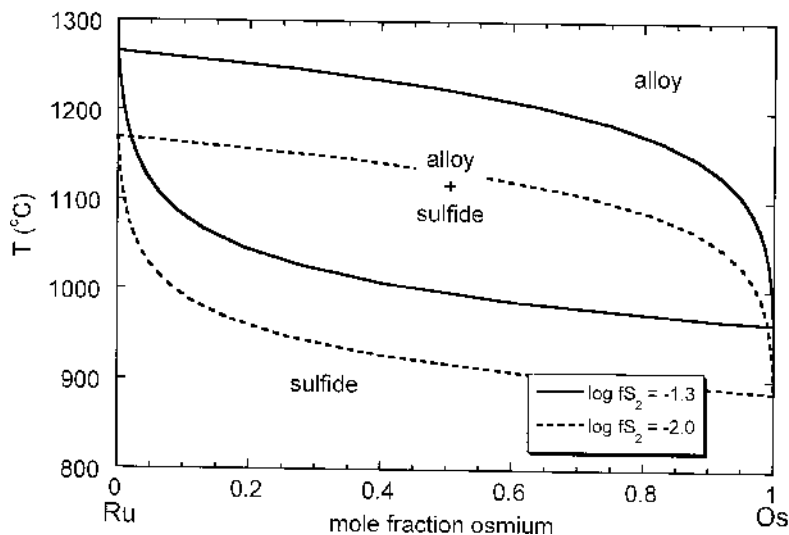

FIG. 1. Phase relations for the binary system Ru–Os as functions of temperature and sulfur fugacity. Phase relations were calculated using the thermodynamic data compiled in Barin (1995) with the assumption of ideal mixing in the solid phase. Note that for a given bulk-composition within the phase field for alloy + laurite, the alloy is always more Os-rich than the coexisting laurite, with both phases becoming more Os-rich with decreasing temperature or increasing fugacity of sulfur.

of Os (or Ir) to a Ru-bearing system. Also, these calculations predict a phase field of sulfide + alloy, with the alloy composition being significantly richer in Os (or Ir), relative to Ru, than the coexisting sulfide. All of these predictions are borne out in our experimental results.

Experimental technique

Two sets of experiments were performed, the first containing mixtures of synthetic basaltic glass (401 diabase from Roeder & Reynolds 1991), forsteritic olivine and Ru metal, whereas the second set (prefixed by "f" in Tables 1–3) contained glass, olivine and an Fe–Ni–S mix (*i.e.,* sulfide melt) doped with Ru–Ir–Os–Pt–Pd metals (each added in subequal proportions). Samples were contained in crucibles fabricated from megacrysts of San Carlos (Arizona) olivine (SCO) and SCO powder was added to each experiment to prevent the melt from migrating out of the crucible at run conditions. The basaltic glass was prepared by repeated grinding and fusion of reagent-grade oxides and carbonates, whereas the sulfide melt was prepared by grinding Fe, Ni, and S powder in ethanol, drying, then doping with the metals, and regrinding. In a typical experiment, basaltic glass (40–80%), olivine powder (~20%), Ru metal (~1–2%) or PGE-metal-doped sulfide melt (~40%) were premixed, and ~70 mg of the basalt–olivine–metal or sulfide mixture was packed into an olivine crucible.

All experiments were performed using a vertical tube furnace modified for control of $f(O_2)$ and $f(S_2)$ by gas mixing. Details of the furnace configuration can be found in Brenan & Caciagli (2000). Experiment temperatures were monitored using a ceramic-sheated Pt–Pt10%Rh thermocouple calibrated against the melting point of gold. A specific gas fugacity was obtained using mixtures of CO, CO_2, and SO_2 in proportions calculated using the "COSHmix" computer program (courtesy of Dr. Victor Kress). As described in Kress (1997), the program uses RAND free-energy minimization of data from JANAF thermodynamic tables to calculate the equilibrium speciation of the gases at high temperature and one atmosphere. Precise control of gas mixtures was achieved using calibrated flow meters, and the $f(O_2)$ predicted from mixing ratios was checked using solid oxide buffers. The range of sulfur and oxygen fugacities (log values) investigated in this study is –2.7 to –1.3 and –10 to –8, respectively. For comparison, the range in (log) $f(S_2)$ and $f(O_2)$ calculated for terrestrial basaltic magmas is –1.8 to +0.8 and –11 to –7.5, respectively (Wallace & Carmichael 1992).

Experiments were initiated by first placing the loaded olivine crucible into a silica glass holder, then suspending this assembly from a silica glass hanger withdrawn to the top of the furnace tube. The furnace was then sealed, and gas flow was commenced. After 20–30 minutes, the sample was slowly lowered into the hot spot (over the course of 30 minutes), and remained there for durations of 1 to 5 days. Experiments were terminated by removing the bottom furnace seal and quickly lowering the sample into an ice-water mixture. A summary of experiment conditions and run products is provided in Table 1.

ANALYTICAL METHODS

Run products were mounted in epoxy either "as is" or as crushed fragments. Mounted samples were prepared for observation and electron-microprobe analysis by grinding with successively finer SiC grit, then either 1 and 0.3 μm alumina or diamond paste, followed by a final polish using colloidal silica. Individual phases were analyzed using the Cameca SX–50 electron microprobe (EMP) at the University of Toronto. Analyses employed an accelerating voltage of 20 kV for sulfides and alloys, and 15 kV for silicate glasses. Platinum-group minerals were analyzed using a focused beam, whereas a 15 μm defocussed beam was used to obtain compositions of silicate and sulfide melt. An 80 nA beam was used for PGM analyses, with 20–60 second count-times on each X-ray peak. Analyses of sulfide melt employed two beam conditions: 20 nA, 5 seconds on peak for Fe, Ni and S, and

TABLE 1. SUMMARY OF EXPERIMENT CONDITIONS AND
RUN-PRODUCT PHASES

Expt.	Duration (hours)	Temperature (°C)	log $f(O_2)$	log $f(S_2)$	Gas-flow rate (cm³/min) CO–SO₂–CO₂	Alloy[2]	Laurite
Sulfide-liquid-undersaturated experiments							
Ru1	12	1300	–9.0	–2.1	27–4.5–42	x	
Ru4	65	1203	–9.1	–2.0	8–6–13.5		x
Ru5	16	1250	–9.0	–2.0	2.6–1–5		x (dc)[3]
Ru8	23	1238	–9.0	–2.0	7.4–3.7–13.6		x (dc)
Ru10	168	1200	–9.1	–2.0	8–6–13.4		x (dc)
Sulfide-liquid-saturated experiments							
Ru7	19	1248	–10.0	–2.7	19–1.4–65.4		x
RuA	68	1200	–9.1	–2.0	8–6–13.5		x
fRu1	45	1200	–9.1	–2.0	8–6–13.5	x	x
fRu2	120.5	1200	–9.1	–2.0	8–6–13.5	x	x
fRu3	72	1250	–8.1	–1.9	3.6–5–0	x	x
fRu4a	73	1300	–9.0	–1.2	10.2–4.5–0	x	
fRu4b	73	1300	–9.0	–1.2	10.2–4.5–0	Assumed[4]	
fRu5rev (fRu4b)[5]	70	1250	–9.4	–1.3	10.2–5–0	x	x
fRu5	70	1250	–9.4	–1.3	10.2–5–0	x	x
fRu7a	79	1200	–9.9	–1.2	10.2–5–0	x	x
fRu7b	79	1200	–9.9	–1.2	10.2–5–0	Assumed	Assumed
fRu8rev (Ru7b)[5]	78	1280	–9.2	–1.2	10.2–4.8–0	x	
fRu9	74	1200	–9.1	–2.0	8–6–13.5	x	x
fRu11	114	1250	–8.1	–1.9	3.6–5–0	x	x
fRu15	114	1200	–9.1	–2.0	8–6–13.5	x	x
fRu16	114	1200	–9.1	–2.0	8–6–13.5	x	x

Notes: 1) Experiments with "f" prefix were doped with Ru–Ir–Os–Pt–Pd mixture, all others contained Ru as sole PGE additive. 2) Denotes phase(s) present. 3) Laurite in state of partial decomposition, although interpreted to be stable during the experiment (see text). 4) Phases were assumed to be present based on result from duplicate experiment. 5) Experiments fRu4b and fRu7b were re-run as fRu5rev and fRu8rev, respectively

80 nA, 20–60 seconds on peaks for the PGE. Oxygen determinations in the sulfide melt relied on peak integration using an ODPB pseudocrystal. Analyses of the silicate melt also used two beam conditions: 10 nA, 5 seconds for major elements, and 80 nA, 60 seconds for sulfur. X-ray lines used to determine PGE concentrations were: Ru$L\alpha$, Os$L\alpha$, Ir$L\alpha$, Pt$L\alpha$, and Pd$L\alpha$; corrections for X-ray overlap were employed for Ru$L\alpha$ on Pd$L\alpha$. For sulfide and alloy analyses, we used pure metals, pentlandite for Fe, Ni, and S, and hematite for oxygen as standards for the PGE. For silicate glasses, a basalt glass was used to standardize most major elements, and pentlandite for Ni and S. In all cases, raw counts were converted to concentrations using a modified ZAF correction routine. As a check on the success of the overlap corrections, and to confirm the spectrometer positions for background measurement, we used our analytical routine to determine the compositions of the PGE metal standards and PGE abundances from experiment RuA, which was doped with Ru as the sole PGE. Reported minimum-detection limits for the PGE are based on these tests.

Representative compositions of silicate melt are provided in Table 2, a summary of laurite, alloy and sulfide liquid compositions is provided in Table 3, and calculated mineral – sulfide melt partition coefficients are reported in Table 4. In some samples, alloy or laurite is noted as being present (on the basis of optical identification), but no analyses have been done. We encountered this problem in only two instances, either because mineral grains produced in the experiment were too small to be analyzed (alloy in fRu7) or too sparse in number (laurite in fRu5rev), such that they were initially identified, but not observed upon further polishing for EMP analysis.

RESULTS

Textural observations of run products

Representative textures from run products are provided in Figures 2 and 3. All experiments to which ex-

cess sulfide melt was added were found to contain spherical globules of immiscible sulfide liquid. With the exception of experiment Ru7, immiscible sulfide liquid was absent in all experiments containing a sulfide-free starting material. The presence of sulfide liquid in Ru7 is probably a result of the low $f(O_2)$ imposed on that experiment, inasmuch as reduced $f(O_2)$ results in a decrease in the sulfur fugacity required to induce sulfide–liquid saturation (data summarized in Carroll & Webster 1994). We initially had difficulty in interpreting the relative stabilities of laurite and Ru alloy in sulfide–liquid-undersaturated experiments owing to modification of the high-temperature phase assemblage during quenching. In several instances, we observed fine-grained, porous aggregates of Ru alloy near the silicate melt – vapor interface, whereas laurite crystals were found elsewhere in the same samples. We finally concluded that this texture developed during the quenching process, as careful examination of some samples revealed laurite crystals near the melt – vapor interface in a state of partial decomposition (Fig. 2). We interpret this tex-

TABLE 2. REPRESENTATIVE COMPOSITIONS* OF SILICATE MELT

	Ru4 (n = 16)	Ru7 (n = 14)	fRu1 (n = 9)	fRu7 (n = 14)
SiO₂ wt%	55.49(0.30)[1]	55.03(0.36)	38.34(0.58)	45.38(0.20)
TiO₂	1.76(0.08)	1.67(0.07)	1.56(0.15)	1.72(0.05)
Al₂O₃	14.92(0.11)	14.25(0.12)	13.49(0.43)	14.51(0.10)
FeO	8.11(0.14)	8.06(0.10)	29.88(0.89)	19.93(0.29)
MgO	7.54(0.10)	9.31(0.07)	5.96(1.23)	6.89(0.09)
CaO	9.46(0.10)	8.81(0.09)	8.46(0.43)	8.94(0.12)
Na₂O	2.66(0.07)	2.65(0.06)	1.89(0.07)	1.87(0.05)
Cr₂O₃	0.09(0.07)	0.22(0.18)	0.01(0.01)	0.02(0.02)
MnO	0.05(0.03)	0.04(0.03)	0.04(0.01)	0.07(0.03)
NiO	0.02(0.02)	0.01(0.02)	0.07(0.02)	0.03(0.03)
S ppm	232(30)	1076(45)	5223(339)	2738(65)
total	100.16	100.31	101.01	100.05

* Results of electron-microprobe analyses. 1) number in parentheses is one standard deviation based on n analyses.

TABLE 3a. COMPOSITION* OF LAURITE

	n	Fe	Ni	S	Os	Ir	Ru	Pt	Pd	total
RuA	18	0.29(0.14)[1]	0.12(0.09)	37.82(0.33)	<0.212	<0.235	61.18(0.65)	<0.27	<0.22	99.68
fRu1	12	0.28(0.11)	0.15(0.06)	37.00(0.24)	<0.21	0.76(0.45)	60.56(0.41)	<0.27	<0.22	99.08
fRu2	12	0.15(0.08)	0.15(0.05)	37.10(0.13)	<0.21	1.01(0.58)	60.28(0.52)	<0.27	<0.22	99.06
fRu3	10	0.62(0.29)	0.56(0.31)	37.52(0.20)	<0.21	0.25(0.19)	60.57(0.46)	<0.27	<0.22	99.94
fRu5	5	0.85(0.33)	0.21(0.11)	37.48(0.18)	0.33(0.17)	1.21(0.59)	59.89(0.54)	<0.27	<0.22	100.27
fRu7	13	0.71(0.34)	0.19(0.06)	37.32(0.98)	<0.21	2.20(0.90)	59.61(0.82)	<0.27	<0.22	100.52
fRu9	17	0.49(0.08)	0.15(0.04)	37.50(0.09)	0.47(0.23)	0.79(0.20)	60.31(0.30)	<0.27	<0.22	99.85
fRu11	8	0.51(0.33)	0.38(0.32)	37.39(0.17)	<0.21	0.47(0.51)	60.17(0.55)	<0.27	<0.22	99.16
fRu15	8	0.55(0.35)	0.25(0.23)	37.28(0.26)	<0.21	0.49(0.29)	61.07(0.89)	<0.27	<0.22	99.72
fRu16	8	<0.04	<0.05	36.93(0.27)	<0.21	0.66(0.07)	60.24(0.46)	<0.27	<0.22	98.16

Notes: 1) The number in parentheses is one standard deviation based on n analyses. 2) The minimum detection limit is based on 2-sigma above background. * Electron-microprobe data (wt% element).

TABLE 3b. COMPOSITION* OF THE ALLOY PHASE

	n	Fe	Ni	Os	Ir	Ru	Pt	Pd	total
fRu1	7	1.71(0.68)	0.50(0.35)	13.04(4.82)	27.47(16.66)	55.00(10.80)	3.80(1.21)	<0.22	101.70
fRu2	13	1.20(0.33)	0.30(0.13)	11.07(6.96)	32.21(11.26)	54.07(5.16)	3.25(0.58)	<0.22	102.12
fRu3	15	1.04(0.25)	0.44(0.19)	10.80(3.72)	23.37(9.48)	62.53(11.85)	2.97(0.76)	<0.22	101.18
fRu4	9	1.15(0.27)	0.22(0.11)	21.35(5.05)	29.06(5.47)	48.04(2.60)	1.51(0.07)	<0.22	101.36
fRu5	12	1.43(0.52)	0.36(0.36)	20.28(10.64)	33.40(10.67)	45.02(1.58)	1.49(0.29)	<0.22	102.12
fRu5rev	10	0.92(0.12)	0.21(0.08)	28.63(2.17)	31.38(1.41)	39.86(3.00)	1.16(0.09)	<0.22	102.17
fRu8rev	11	0.79(0.13)	0.18(0.07)	16.16(0.98)	16.30(1.02)	66.56(1.62)	2.01(0.13)	<0.22	102.00
fRu9	5	2.21(0.34)	0.29(0.06)	2.10(1.78)	53.15(4.38)	42.10(3.26)	2.65(0.33)	<0.22	102.50
fRu11	5	0.90(0.11)	0.32(0.12)	13.55(9.75)	31.49(8.56)	51.74(15.77)	3.93(1.48)	<0.22	101.93
fRu15	7	1.19(0.32)	0.38(0.18)	16.30(6.26)	19.87(6.71)	59.30(1.71)	3.83(0.17)	<0.22	100.89
fRu16	2	2.75	0.25	14.53	19.77	58.07	3.03	<0.22	98.98

Notes: as per Table 3a.   * Electron-microprobe data (wt% element).

TABLE 3c. COMPOSITION* OF SULFIDE LIQUID

	n	Fe	Ni	S	O	Os	Ir	Ru	Pt	Pd	total
RuA	10	37.45(2.17)	25.75(2.35)	30.38(0.57)	1.66(0.85)	<0.20	<0.24	5.67(0.59)	<0.27	<0.11	100.98
fRu1	17	40.84(4.43)	20.63(4.74)	29.70(2.31)	2.70(2.99)	<0.20	<0.24	3.41(0.63)	0.74(0.69)	2.71(1.16)	100.82
fRu2	18	35.71(1.61)	20.24(1.86)	29.75(0.97)	2.12(0.75)	0.38(0.05)	<0.24	8.26(0.84)	1.72(1.48)	2.86(0.74)	101.09
fRu3	19	31.70(3.04)	24.97(3.53)	27.59(1.58)	1.56(0.39)	<0.20	<0.24	7.42(2.25)	3.31(0.66)	3.22(0.97)	100.23
fRu4	13	43.97(1.35)	12.67(0.81)	29.99(0.77)	2.93(0.48)	<0.20	<0.24	7.60(0.63)	1.19(0.75)	1.74(0.40)	100.50
fRu5	20	43.40(1.43)	12.20(0.92)	30.22(1.14)	2.31(0.48)	<0.20	<0.24	8.60(0.44)	1.73(1.15)	1.72(0.34)	100.53
fRu5rev	26	39.33(1.71)	15.50(1.54)	29.84(1.09)	1.93(0.68)	0.38(0.05)	0.47(0.19)	8.54(0.70)	2.17(1.32)	2.44(0.77)	100.60
fRu7	20	51.75(1.21)	9.59(0.98)	30.71(0.61)	3.09(0.47)	<0.20	0.57(0.14)	2.45(0.26)	1.25(0.82)	1.06(0.28)	100.54
fRu8rev	25	36.80(0.73)	14.89(0.73)	30.80(0.54)	1.45(0.30)	0.45(0.05)	<0.24	13.00(1.07)	0.57(0.32)	2.00(0.41)	99.97
fRu9	16	39.06(5.03)	22.22(4.85)	29.84(0.82)	2.15(0.99)	<0.20	<0.24	2.83(1.00)	1.37(0.66)	2.96(1.72)	100.57
fRu11	12	29.71(1.11)	24.59(0.83)	30.17(0.66)	0.90(0.31)	<0.20	<0.24	10.26(1.62)	1.03(0.75)	3.81(0.36)	100.66
fRu15	16	36.45(1.44)	20.24(2.02)	28.99(1.30)	2.00(0.87)	<0.20	<0.24	7.98(1.03)	1.41(0.60)	2.61(0.52)	99.73
fRu16	9	59.13(1.36)	5.32(1.32)	25.02(1.10)	7.92(1.39)	<0.20	<0.24	0.95(0.51)	0.31(0.29)	0.74(0.29)	99.53

Notes: as per Table 3a.   * Electron-microprobe data (wt% element).

ture as arising from the brief reduction in sulfur fugacity experienced by the sample during the quench.

In the sulfide-liquid-undersaturated experiments, laurite crystals occur as clusters of euhedral to anhedral grains (Fig. 2), whereas laurite is present as isolated euhedral crystals in those experiments containing an immiscible sulfide liquid (Figs. 3A, C). In these latter experiments, laurite is invariably preferentially wetted by the sulfide liquid. Crystals of laurite from experiments fRu3 and fRu9 [1250°C, log $f(S_2)$ = –2] are skeletal in form (Fig. 3B), in contrast to the euhedral crystals produced in an experiment at the same temperature, but higher $f(S_2)$ [fRu5, log $f(S_2)$ = –1.3, Fig. 3C]. Euhedral to subhedral grains of Ru–Os–Ir alloy are present in all experiments containing the multi-PGE mixture, and alloy grain-sizes decrease with either a reduction in temperature or an increase in sulfur fugacity. Although

some alloy grains are observed in several of the sulfide-liquid-undersaturated experiments, this material was in every case interpreted to be a product of quench-induced decomposition of laurite. Subhedral clusters of what appears to be *stable* Ru alloy are present only in the experiment run at 1300°C.

Assessment of equilibrium

Several observations suggest that near-equilibrium phase assemblages and compositions were achieved in our experiments. First, mineral assemblages were reproduced using either metals or alloys or laurite + alloy as the initial PGE-bearing phases. Most experiments in the "f" series started with a mechanical mixture of PGE metals, whereas experiments fRu5rev and fRu8rev used the run products from experiments containing a single
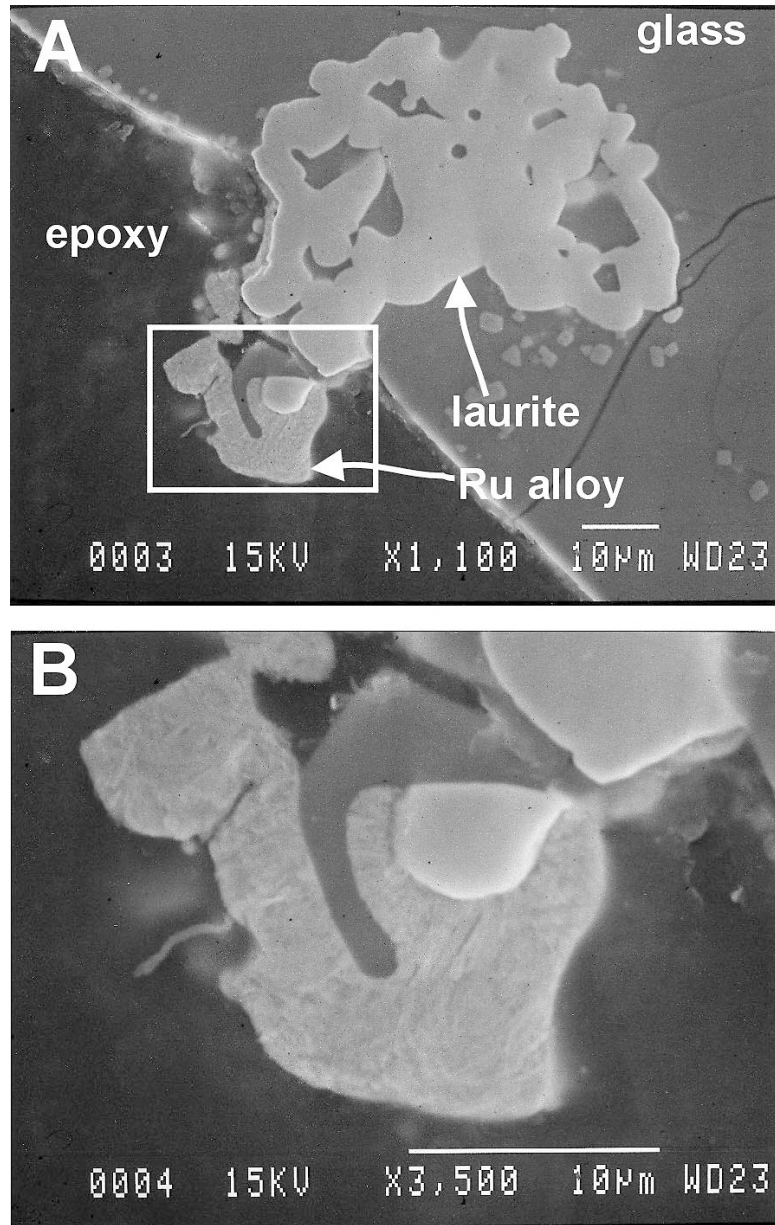
FIG. 2.   Secondary electron image of a portion of the run product from experiment Ru4. This image was taken at the melt–vapor interface (void space occupied by the latter phase now filled with epoxy). Laurite in direct contact with the vapor has partially decomposed to alloy (close-up in B). This texture is interpreted to be a consequence of the reduction in sulfur fugacity experienced by the sample during the quenching process.
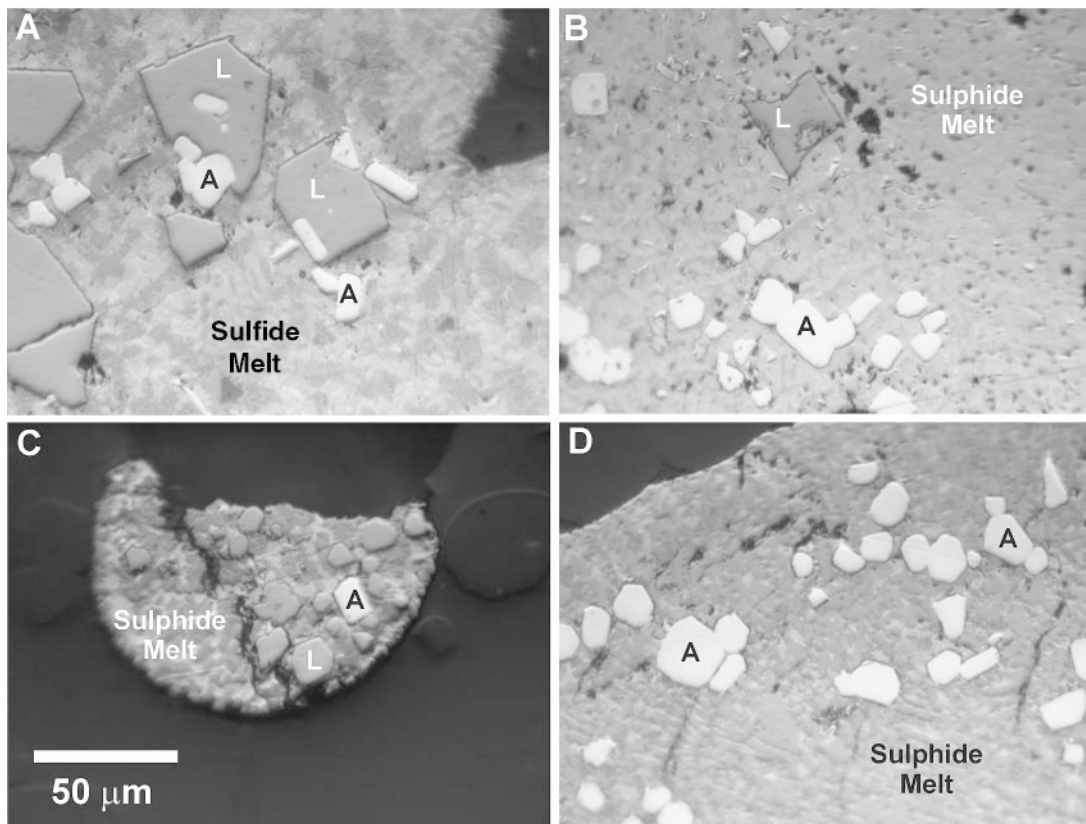
FIG. 3.   Reflected-light photomicrographs (plane-polarized light) of run products from experiments containing immiscible silicate and sulfide melts (L: laurite, A: Ru–Ir–Os alloy; all images taken at the same magnification). A) fRu1 [45 hrs, 1200°C, log $f(S_2)$ = – 2.0], B) fRu3 [73 hrs, 1250°C, log $f(S_2)$ = –1.9], C) fRu5 [70 hrs, 1250°C, log $f(S_2)$ = –1.3], D) fRu4a [73 hrs, 1300°C, log $f(S_2)$ = –1.3].

Ru–Os–Ir alloy or alloy + laurite, respectively, as the PGE-bearing minerals. In the second part of the latter experiments, samples were subject to conditions in which alloy was unstable with respect to alloy + laurite (fRu5rev) or laurite + alloy was unstable with respect to alloy (fRu8rev), as judged from previous "forward" experiments involving mixtures of metals. In each case, the phase assemblages of the "forward experiment" were reproduced. We did recognize some residual material from the forward experiments, however, in these reversals. For example, some grains of alloy in experiment fRu8rev are anomalously Ru-rich, with compositions defining a trend that projects back to that of the laurite present in the starting material (Fig. 4).

In addition to reversed assemblages, individual grains of laurite produced in our forward experiments are relatively homogeneous in those cases where mineral grains were large enough for multiple analyses. Figure 5 portrays the results of multiple analyses for iridium across individual crystals of laurite from three different experiments. Occasionally, moderate to severe spikes in Ir (± Os) content were found, which we attribute to X-ray excitation from small inclusions of alloy that have been observed in some grains. Aside from variations due to inclusions, however, individual grains display no systematic core–rim variations and are generally homogeneous. We could not perform the same multiple-point analyses on individual grains of alloy owing to their small size. Analyses of multiple grains did yield some variability (up to 50% or more), which is probably a result of inclusion of some melt in the volume of alloy analyzed (although compositions with appreciable sulfur were excluded from the dataset), and zonation produced owing to the extreme compatibility of Ru, Ir and Os in the alloy phase. Grains of alloy have undergone extensive chemical exchange relative to the starting material, as the initial alloy assemblage contained Pt and Pd, which have been partially (Pt) to completely (Pd) excluded from the final alloy composition (Table 3b), and sequestered by the sulfide liquid.
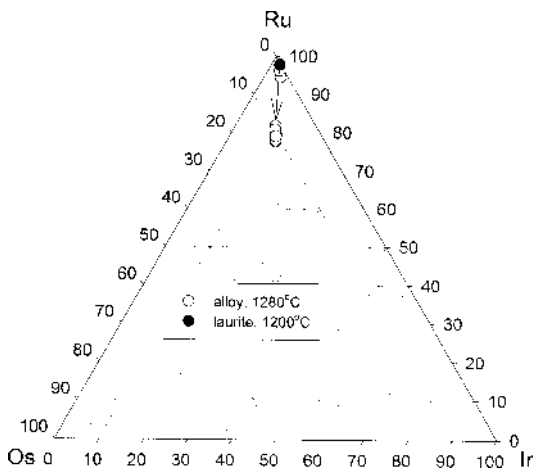
FIG. 4. Triangular diagram (atomic %) depicting the composition of laurite from experiment fRu7a and alloy from fRu8rev. Note that the alloy compositions trend from Ru-rich (similar to laurite) to Ir–Os-rich.

± 30 ppm. For this latter composition, calculations using the Wallace–Carmichael model also indicate that saturation in an immiscible sulfide liquid will not occur until the log $f(S_2)$ increases to a value of –0.8, at which point the melt would contain ~900 ppm dissolved sulfur.

Sulfide melt compositions

Sulfide melt compositions are Fe- and Ni-rich, with sulfur and oxygen contents of ~25–31 and ~1–8 wt%, respectively. The melt with the lowest sulfur and highest oxygen contents corresponds to the one experiment in which we added extra iron to the Fe–Ni–PGE–S component. All other experiments contain the same Fe–Ni–PGE–S component in their starting composition, so variations in their Fe content correspond to either variations in initial sulfide:silicate melt ratio, $f(O_2)/f(S_2)$ ratio (which dictates the sulfide melt – silicate melt partitioning of Fe), or the iron content of the olivine crucible (which is considered to vary somewhat, as judged by color differences among crucibles). The PGE content of the sulfide melts produced are uniformly low for iridium and osmium (<0.6 wt% in all cases), whereas

Silicate melt compositions

We analyzed glasses from a representative suite of experiments to assess their chemical homogeneity and to determine if sulfur contents in the melt are consistent with previous studies. The most distinctive difference in the composition of silicate melts produced is the abundance of FeO. Samples to which the sulfide melt mixture was added (*e.g.,* fRu1, fRu7; Table 2), yielded silicate melts with 20–30 wt% FeO, in comparison to samples that were initially sulfide-free (*e.g.,* Ru4, Ru7), which contain ~8 wt% FeO. This result is clearly a bulk-composition effect, as Fe added to the experiment in the sulfide melt mixture reacts with oxygen in the vapor to form FeO, which dissolves in the silicate melt. Silicate melts with the highest Fe contents also have the highest abundance of dissolved sulfur, which reflects a sulfur-solution mechanism involving association with Fe in the melt (Carroll & Webster 1994). Haughton *et al.* (1974) defined the S–FeO variation for a sulfide-liquid-saturated basalt similar to the composition employed in this study, and a comparison of results is portrayed in Figure 6. Our results are in very good agreement with the sulfide-saturation curve derived from their experiments, with all of our sulfide-saturated compositions plotting near or on the curve, and the undersaturated composition plotting below the curve. The solubility model of Wallace & Carmichael (1992) describes the sulfur content of a silicate melt coexisting with a S-bearing vapor at a particular T, $f(S_2)$ and $f(O_2)$. Using this model, a concentration of 316 ± 84 ppm sulfur is calculated for the sulfide-liquid-undersaturated melt of experiment Ru4, which is within error of the measured value of 232
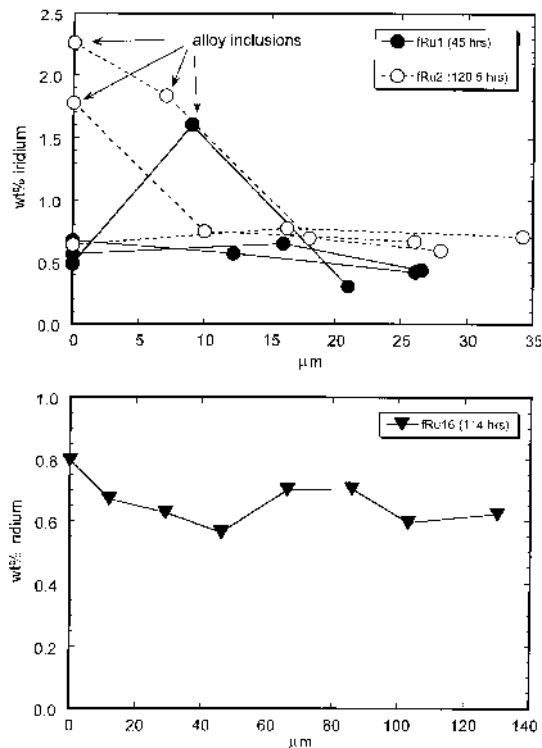

FIG. 5. Iridium concentration profiles across single crystals of laurite from various run-products. The spikes in iridium concentration are interpreted to be the result of X-ray excitation from small inclusions of alloy.
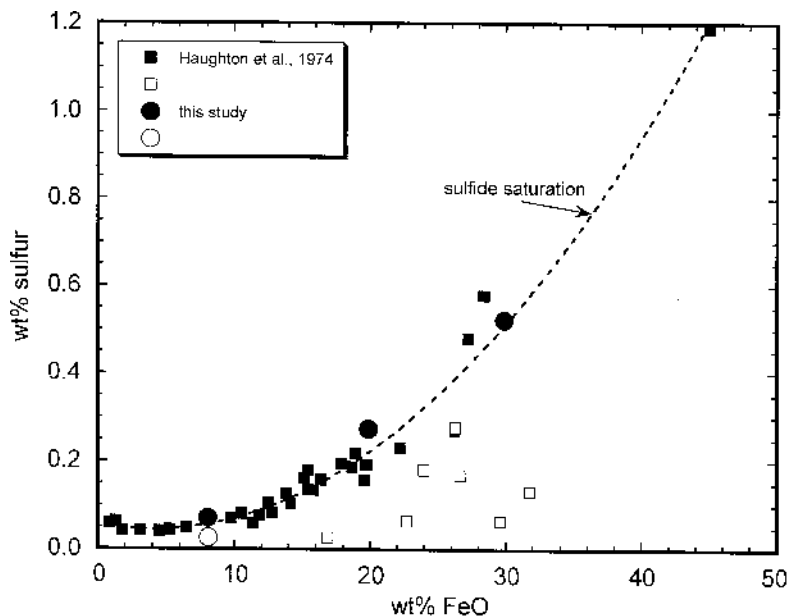
FIG. 6.   Variation in the sulfur content of silicate melt coexisting with S-bearing vapor as
a function of FeO content. Compositions are those measured in this study, and from
Haughton *et al.* (1974), and were synthesized at 1200°C over a range of $f(O_2)$ and $f(S_2)$.
Filled symbols correspond to samples saturated in an immiscible sulfide liquid, whereas
open symbols are sulfide-free. The dashed line is regressed from data of Haughton *et al.*
(1974) and corresponds to the sulfide saturation-surface for melts of variable FeO con-
tent. Note that experiment Ru7 was done at 1248°C, and the measured S content has
been recalculated to 1200°C using the T-dependence of S solubility determined by
Richardson & Fincham (1956).

Pt and Pd contents are ~0.5–4 wt%, and Ru contents
were found to be ~1–13 wt% (Table 3c). Given that all
experiments were saturated in a Ru–Os–Ir-rich alloy, the
low Os and Ir contents of sulfide liquids reflect the low
solubility of these elements in the melt phase. Pd is ex-
cluded from both laurite and Ru–Os–Ir alloy (Table 3a,
b), and thus variations in the Pd content of sulfide liq-
uids probably reflects differences in the abundances of
this element in the material added to an experiment. A
similar explanation is true for Pt, although the Pt con-
tent of the sulfide melt will be controlled to some extent
by the abundance of Ru–Os–Ir alloy, owing to the mod-
erate levels of Pt measured in this phase (~3 wt%;
Table 3b). Relative abundances of PGE in sulfide melt
coexisting with Ru–Os–Ir alloy are generally consistent
with previous determinations. For example, Fleet &
Stone (1991) reported results from experiments at 1 bar
and 1200°C that produced sulfide melt with <1 wt% Ir
and <0.1 wt% Os coexisting with alloys containing 77–
88 wt% Ir and 97 wt% Os. The Pt and Pd content of
their melts were similar to amounts added to the start-
ing material, consistent with the high solubilites for
these elements documented in our experiments. Peach

& Mathez (1996) measured somewhat higher Ir concen-
trations (~4 wt%) in sulfide melt equilibrated with Ir–
Fe alloy (~90% Ir) at 0.8 GPa and 1450°C, which may
reflect differences in alloy composition or the higher
temperature.

For experiments conducted at the same temperature
and $f(S_2)$, but different durations, we observed a small,
but systematic decrease in the Fe content of the sulfide
liquid, and a complementary increase in Ru content
(Fig. 7). In addition, with increasing temperature, but at
constant $f(S_2)$, the Fe content of the sulfide liquid also
decreases, whereas the Ru content increases (Fig. 7). Al-
though the change in melt Fe content with run duration
is probably a result of continued Fe–Mg exchange be-
tween the olivine crucible and the sample, we expected
that the Ru content of the melt would be buffered by the
presence of the Ru-rich sulfide and alloy phases, whose
compositions are roughly fixed. The covariation of Fe
and Ru in the sulfide liquid may be the result of a de-
crease in the activity coefficient for Ru with decreasing
Fe content of the melt. We tested this hypothesis by
conducting an experiment in which the added Fe–Ni–
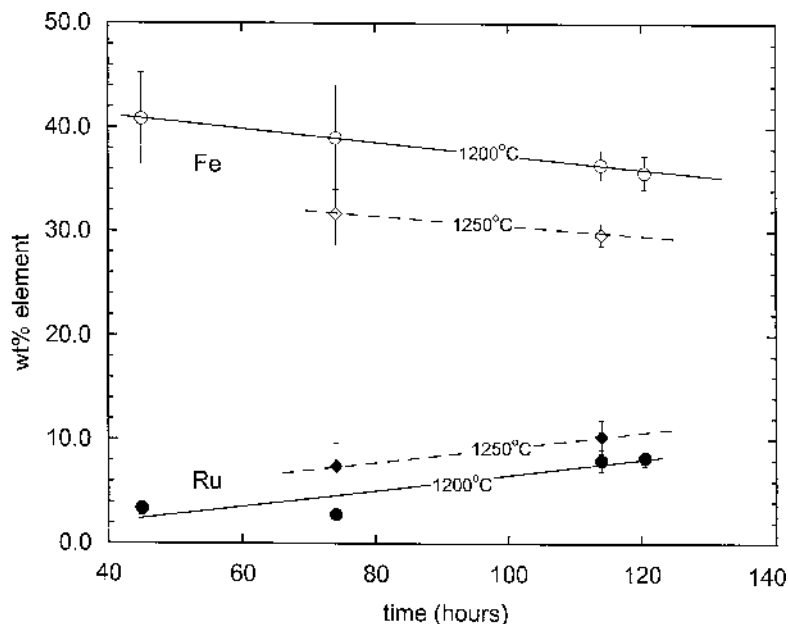PGE–S component was Fe-rich (fRu16), and, as ex-

FIG. 7. Variation in composition of sulfide melt (wt% Fe and Ru) as a function of run duration for experiments at 1200 and 1250°C and log $f(S_2) = -2$. Note that the Fe and Ru contents of the melt vary in a complementary way.

pected, the Ru content of the resulting sulfide liquid was significantly lower than that of experiments with lower Fe contents, but similar duration (*cf.* fRu15 and fRu16 with ~8 and ~1 wt% Ru, ~36 and ~59 wt% Fe, respectively, in the sulfide liquid).

Compositions of laurite and alloy

It is notable that in all of the experiments conducted, the composition of laurite corresponds to nearly pure RuS_2, with low concentrations of Ir and Os, and undetectable levels of Pt and Pd (Table 3a). Alloy compositions are significantly enriched in Os and Ir relative to laurite, and contain low, but uniform levels of Pt, and undetectable Pd. The relative exclusion of Pt and Pd from the alloys produced in our experiments is also in agreement with the compositions of alloys from the experiments of Fleet & Stone (1991). Both laurite and alloy are Fe- and Ni-poor, with the alloy having somewhat higher abundances of both of these elements (Table 3a, b). Figures 8 and 9 portray the compositions of coexisting laurite and alloy in terms of the relative abundances of Ru, Ir and Os (atomic %), as functions of temperature and $f(S_2)$, respectively. The variation in alloy composition (and tieline position) for experiments run at a single set of conditions results from differences in the bulk compositions of the samples, which is prob-

ably a result of the "nugget effect" on the PGE distribution within the starting material. As shown in Figure 8, at 1200°C and log $f(S_2) = -2$, coexisting alloy and laurite define a compositional field within which both PGM will crystallize. The field extends to ~60 at.% Ru for Ir-rich compositions, and ~75 at.% Ru for more Os-rich bulk compositions. Increasing temperature appears to have little effect on the extent of the two-phase field, as alloy compositions at 1250°C scatter near those produced at 1200°C. The Os–Ir-rich character of the alloy coexisting with the Ru-rich laurite is in accord with the phase relations portrayed in Figure 1. In all cases, alloys are too Ir-poor to intersect the miscibility gap (> 50 at.% Ir) defined by Harris & Cabri (1991).

Maximum thermal stability of laurite

In order to determine if laurite can coprecipitate with minerals like chromian spinel on the basalt liquidus, and thus become an included phase, the maximum thermal stability of laurite was assessed by monitoring its presence or absence at a particular condition of T and $f(S_2)$. For experiments at log $f(S_2) = -2$ doped with only Ru, laurite is present in the run products up to 1250°C, and absent in the the experiment at 1300°C, thus bracketing the thermal stability to be ~1275 ± 25°C. In the experiments doped with multiple PGE, laurite was found to

coexist with Ru–Os–Ir alloy up to 1250°C at log $f(S_2) =$ –2 and –1.3, and is absent from the run products in experiments at 1280 and 1300°C at log $f(S_2) =$ –1.3, thus bracketing the thermal stability to be ~1265 ± 15°C. The presence of skeletal laurite in the experiments at 1250°C and log $f(S_2) =$ –2 may suggest that the maximum thermal stability of laurite is close to 1250°C at this $f(S_2)$. These results are broadly in accord with calculated phase-relations portrayed in Figure 1, in that the maximum thermal stability of near-end-member laurite is near 1300°C at log $f(S_2) =$ –1.3. However, our results differ from the calculated thermal stability of laurite at log $f(S_2) =$ –2, in which the predicted temperature of breakdown is ~1180°C. We have found, however, that even small uncertainties in the thermodynamic data for these minerals will have a relatively significant effect on their calculated thermal stability, which probably accounts for this discrepancy. The most important result from this analysis is that laurite is found to be stable at liquidus temperatures of the basalt and values of $f(S_2)$ that are both 1) at the *low end* of estimates for natural magmas, and 2) at *and below* those required for saturation in immiscible sulfide liquid.

Partitioning of PGE among alloy, laurite and sulfide or silicate liquid

Table 4 summarizes calculated laurite– and alloy – sulfide melt partition coefficients for Fe, Ni, Os, Ir, Ru, Pt and Pd; values are plotted in Figures 10A and B. In some cases, the PGE concentration in one of the phases of interest is too low to be detected, and consequently
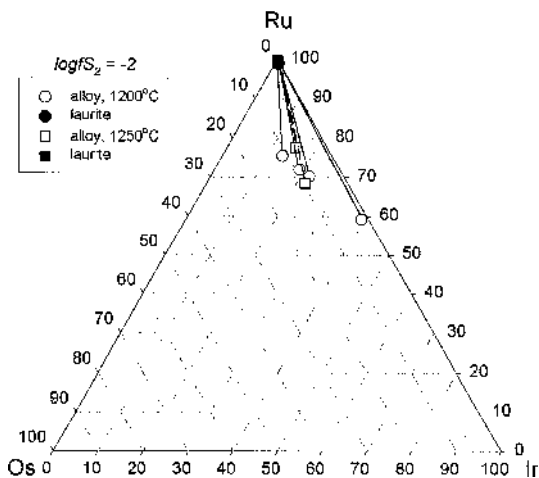

FIG. 8. Triangular diagram (atomic %) depicting the average compositions of coexisting laurite and alloy from experiments at constant $f(S_2)$ [log $f(S_2) =$ –2], but variable temperature (1200, 1250°C). Tielines connect coexisting laurite and alloy.
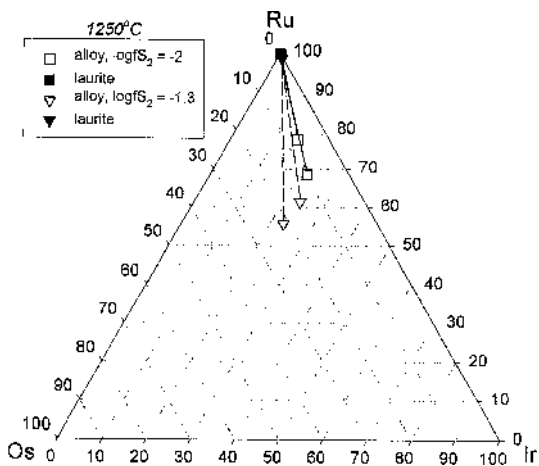

FIG. 9. Triangular diagram (atomic %) depicting the average compositions of coexisting laurite and alloy from experiments at constant temperature (1250°C), but variable $f(S_2)$ [log $f(S_2) =$ –1.3 and –2]. Tielines connect coexisting laurite and alloy.

only minimum (melt < MDL) or maximum (laurite or alloy < MDL) partition-coefficients could be determined. Note that the calculation of a Nernst (weight ratio) partition coefficient for elements that are major constituents of laurite or alloy (*i.e.,* Ru in laurite and Ru, Os, Ir in alloy) is of limited use for geochemical modeling, inasmuch as the composition of the solid phase is relatively fixed; as a result, partition coefficients are a sensitive function of melt composition. Results are presented in this manner simply to show the relative degrees of retention of these elements in the solid phase for a melt having broadly similar Fe, Ni and PGE abundances. Relative to the sulfide liquid, both laurite and alloy exclude Fe, Ni, and Pd, whereas both phases concentrate Ir and Ru. The behavior of Pt is somewhat different in that laurite excludes Pt and Pd to a similar degree (both mineral/melt D being <<1), whereas the alloy phase exhibits a preference for Pt (D of ~1 to ~10), while excluding Pd (D of <0.3). Estimates for the laurite/ melt D for osmium yielded values that are ≥2 and ≥0.6, although the former values might be somewhat high, as grains of laurite formed in these experiments are relatively small, and the electron beam may have impinged on some inclusion material. In contrast to the near-unity laurite–melt D for Os, alloy – sulfide melt partition-coefficients for Os are uniformly high (>30). On the basis of phase relations portrayed in Figure 1, we expect that the laurite–melt D for osmium (and iridium) will increase significantly with falling temperature.

We have not, as yet, analyzed the coexisting silicate melt from our experiments for PGE, but can provide estimates for laurite – and alloy – silicate melt parti-

TABLE 4. CALCULATED LAURITE – SULFIDE MELT AND ALLOY – SULFIDE MELT PARTITION COEFFICIENTS

	phase	Fe	Ni	Os	Ir	Ru	Pt	Pd
fRu1	laurite	0.0069(0.0028)	0.0073(0.0034)	ND	>3.2	18(3)[2]	<0.37	<0.081
	alloy	0.042(0.017)	0.024(0.018)	>65	>110	16(4)	5.1(5.1)	<0.081
fRu2	laurite	0.0042(0.0022)	0.0074(0.0026)	<0.55	>4.2	7.4(0.8)	<0.16	<0.077
	alloy	0.034(0.009)	0.015(0.007)	29(19)	>130	6.6(0.9)	1.9(1.7)	<0.077
fRu3	laurite	0.020(0.009)	0.022(0.013)	ND	>1.0	8.2(2.5)	<0.082	<0.068
	alloy	0.033(0.008)	0.018(0.008)	>54	>97	8.4(3.0)	0.90(0.29)	<0.068
fRu4	alloy	0.026(0.006)	0.017(0.009)	>107	>120	6.3(0.6)	1.3(0.8)	<0.13
fRu5	laurite	0.020(0.008)	0.017(0.009)	>1.7	>5.0	7.0(0.4)	<0.16	<0.13
	alloy	0.033(0.012)	0.030(0.030)	>101	>139	5.2(0.3)	0.86(0.60)	<0.13
fRu5rev	alloy	0.023(0.003)	0.014(0.005)	75(11)	67(27)	4.7(0.5)	0.53(0.33)	<0.09
tRu7	laurite	0.014(0.007)	0.020(0.007)	ND	3.9(1.8)	24.3(2.6)	<0.22	<0.21
fRu8rev	alloy	0.021(0.004)	0.012(0.005)	36(5)	>68	5.1(0.4)	3.5(2.0)	<0.11
fRu9	laurite	0.013(0.003)	0.0068(0.0023)	>2.4	>3.3	21(8)	<0.20	<0.074
	alloy	0.057(0.011)	0.013(0.004)	>11	>221	15(5)	1.9(1.0)	<0.074
fRu11	laurite	0.017(0.011)	0.015(0.013)	ND	>1.9	5.9(0.9)	<0.26	<0.058
	alloy	0.030(0.004)	0.013(0.005)	>68	>130	5.0(1.7)	3.8(3.1)	<0.058
fRu15	laurite	0.015(0.010)	0.012(0.011)	ND	>2.0	7.7(1.0)	<0.19	<0.084
	alloy	0.033(0.009)	0.019(0.009)	>82	>83	7.4(1.0)	2.7(1.2)	<0.084
fRu16	laurite	<0.00068	<0.0094	ND	>2.9	62(33)	<0.87	<0.30
	alloy	0.047(0.001)	0.047(0.012)	>73	>82	61	9.8	<0.30

Notes: 1) ND: partition coefficient not determined (concentrations < MDL in both phases).
2) 1σ error in partition coefficient based on combined uncertainties in concentrations for both phases.

tion-coefficients based on published sulfide – silicate melt values. As shown in several studies (Stone *et al.* 1990, Bezmen *et al.* 1994, Fleet *et al.* 1996), sulfide – silicate melt partition-coefficients for the PGE are uniformly high (*i.e.,* ~10^2–10^5), and within the uncertainty of a given dataset, there does not appear to be a systematic difference in partition behavior between the IPGE and the PPGE (see also Peach & Mathez 1996). Thus, we expect that PGM – silicate melt partition-coefficients for the PGE will display the same relative values as those involving sulfide melt, implying that laurite or alloy crystallization will result in a strong preferential uptake of the IPGE into the solid phase relative to coexisting silicate melt.

DISCUSSION AND CONCLUSIONS

Comparison with natural laurite and Ru–Os alloy compositions

Compositions of associated laurite and Ru–Ir–Os alloy from natural samples are provided in Table 5 and projected on the ternary system Ru–Os–Ir (at%) in Figure 11A. In this case, the term "associated" refers to laurite and alloy that occur as touching grains and as spatially proximal inclusions within the same host-mineral grain (invariably chromian spinel) or, in the case of placer deposits (Samar ophiolite only), samples derived from the same rock-formation. In all cases, reported occurrences of associated laurite *and* alloy are from chromitites within ophiolite complexes. The composi-

tional characteristics of natural laurite and alloy are broadly similar to those synthesized in our experiments; both natural and synthetic PGM are low in Pt, Pd, Fe and Ni, with alloys being significantly richer in Pt, Os and Ir, and poorer in Ru, than the associated laurite (Table 5). A comparison of Figure 11A with Figures 8 and 9 reveals, however, that the compositions of natural laurite and alloy tend to be poorer in Ru than compositions produced in our experiments. Indeed, compositions of natural alloy project close to the Os–Ir join in Figure 11A, whereas our synthetic alloy contains no more than ~20 at% Os and ~30 at% Ir. One possible reason for this discrepancy is that the natural laurite–alloy pairs may have crystallized or exchanged at lower temperatures than those employed in our experiments. As shown in Figure 1, for any bulk composition and $f(S_2)$, laurite and alloy formed at the highest temperatures will be Ru-rich; with falling temperature, both laurite and alloy will tend toward more Os-rich (and Ir-rich) compositions. This process requires that the $f(S_2)$ remain constant in order to accommodate the formation of more sulfide as temperature falls. Such a scenario is possible if the alloy and sulfide remain open to sulfur exchange with an external reservoir (*i.e.,* a magma), but cannot occur if the minerals become trapped within growing chromian spinel phenocrysts, which is their most common association. Moreover, for the case of bulk compositions that project into the ternary sytem Ru–Ir–Os, we have found that a reduction in temperature from 1250 to 1200°C had little effect on the compositions of coexisting laurite and alloy. Given that such temperatures are reasonable

FIG. 10. Calculated mineral – sulfide melt partition coefficients for Fe, Ni, Os, Ir, Ru, Pt and Pd. A) Laurite – sulfide melt. B) Alloy – sulfide melt. Open symbols correspond to maximum or minimum partition-coefficients (distinguished by arrow direction), whereas filled symbols denote absolute values.

for the initiation of crystallization of chromian spinel, entrapment of coexisting alloys at the T–$f(S_2)$ conditions of our experiments seems unlikely. However, an increase in $f(S_2)$ of 0.7 log units did result in an increase in the Os and Ir content of both laurite and alloy (consistent with binary phase-relations), which suggests that the natural assemblages probably crystallized at a higher $f(S_2)$ than that imposed on our experiments.

Figure 11B portrays the composition of natural laurite from parageneses that do not contain associated Ru–Ir–Os alloy. Laurite in this case occurs in both lay-

ered intrusions (Stillwater, Bushveld) and in ophiolites, and in nearly all cases, it occurs as inclusions within a chromian spinel host. Although there is some overlap with the laurite compositions portrayed in Figure 11A, those in Figure 11B tend to be both Ir-poor, and trend to more Os-rich compositions, than laurite associated with Ru–Os–Ir alloy. In comparison to laurite produced in our experiments, even the most Ru-rich laurite in Figure 11B contains more Ir and Os than the compositions we have synthesized, again suggesting that $f(S_2)$ during laurite formation and entrapment was higher in nature

TABLE 5. REPRESENTATIVE COMPOSITIONS OF ASSOCIATED LAURITE AND ALLOY FROM OPHIOLITES

| locality	phase	reference	S	Os	Ru	Ir	Rh	Pt	Pd	Ni	Cu	Fe	sum
Tiebaghi, New Caledonia	alloy	1	2.54	8.02	3.6	81.67	0.27	1.51	0.05	1.57	0.36	n.d.	99.59
	laurite		35.73	7.65	43.23	12.38	0.21	n.d.	0.22	0.19	n.d.	n.d.	99.61
Vourinos, Greece	alloy	2	n.d.	58.52	1.02	39.06	0.85	n.d.	0.33	0.08	n.d.	n.d.	99.86
	alloy		0.96	63.74	1.14	33.34	0.49	n.d.	0.01	0.06	n.d	n.d.	99.74
	laurite		34.74	23.1	34.72	5.57	1.21	n.d.	0.49	0.16	n.d.	n.d.	99.99
	laurite		31.96	29.2	30.85	7.14	0.72	n.d.	n.d.	0.12	n.d.	n.d.	99.99
Thetford Mines, Quebec	alloy	3	32.9	21.1	34.9	8.1	1.7	n.d.	n.d.	n.d.	n.d	n.d.	98.7
	laurite		n.d.	61	1.3	37.4	0.3	n.d.	n.d.	n.d.	n.d.	n.d.	100
Samar, Philippines	alloy	4	n.d.	19.31	0.74	73.07	n.d.	6.29	0.16	n.d.	n.d.	0.36	99.93
	alloy		n.d.	55.45	7.31	33.13	n.d.	3.05	0.31	n.d.	n.d.	0.12	99.37
	laurite		30.94	25.53	36.13	6.95	0.63	n.d.	n.d.	n.d.	n.d.	0	100.18
	laurite		31.85	21.54	42.64	3.88	0.65	n.d.	n.d.	n.d.	n.d.	0	100.56
Josephine, Oregon	alloy	5	n.d.	30.67	1.2	47.87	1.7	13.3	n.r.	0.05	n.d.	0.53	95.32
	alloy		n.d.	60.1	2.1	30.83	0.34	2.09	n.r.	n.d.	n.d.	0.5	95.96
	laurite		32.6	16.5	36.96	10.24	n.r.	n.d.	n.r.	0.07	n.d.	0.51	96.88
	laurite		34.45	11.91	44.72	7	n.r.	n.d.	n.r.	0.02	0.02	0.24	98.36

n.d.: not detected; n.r.: not reported. References: 1: Augé (1988), 2: Augé (1985), 3: Corrivaux & Laflamme (1990), 4: Nakagawa & Franco (1997), 5: Stockman & Hlava (1984).

than in our experiments. The trend to Os-rich compositions in the Ojen (Spain) and Othrys (Greece) ophiolites is probably a result of early crystallization and removal of the Ru-rich laurite, as dictated by the binary phase-relations portrayed in Figure 1. Some of the laurite compositions from these latter two ophiolites project into the two-phase field defined by associated laurite and alloy in Figure 11A. Provided that small amounts of Os–Ir alloy have not been overlooked in these samples, this observation suggests that higher $f(S_2)$ prevailed during crystallization in the Ojen and Othrys ophiolites than in those portrayed in Figure 11A.

Data presented in Figure 11C, reported from the Kamuikotan ophiolite belt (Hokkaido, Japan), provide an example of a locality in which alloy is the sole documented host for the IPGE. In this case, most alloy compositions plot within the alloy-only field defined by our experiments, whereas some plot within our experimentally determined two-phase field. This latter observation would suggest that such alloy crystallized at conditions below the $f(S_2)$ defined by our experiments. It is also notable that many of these alloy compositions plot within the two-phase field defined by the associated laurite + alloy in Figure 11A. Again, provided small amounts of laurite have not been overlooked in these samples, this result would indicate a relatively low $f(S_2)$ during crystallization compared to the samples portrayed in Figures 11A or B, as previously concluded by Nakagawa & Franco (1997).

Implications for IPGE/PPGE fractionation in natural magmas

The results of this study show that laurite can be stable at high temperature and at sulfur fugacities within the range recorded by natural mafic magmas. In addition, the compositions of laurite and coexisting alloy are broadly consistent with the compositions of associated laurite and alloy from natural parageneses. Because of the high thermal stability we have documented, these results lend further credence to the notion that laurite can be a primary magmatic phase, and is capable of coprecipitation and subsequent entrapment by other primary liquidus phases, such as chromian spinel (*e.g.,* Merkle 1992, Hiemstra 1979). Although it is not clear to us why chromian spinel appears to preferentially nucleate on coexisting laurite, separate experiments involving chromian spinel – melt partitioning in the presence of alloy and sulfide (Sattari *et al.* 1999) show that chromian spinel commonly includes these phases. Tredoux *et al.* (1995) have emphasized the notion that inclusion of PGM into liquidus phases such as chromite may be a natural consequence of the presence of the PGE as polyatomic aggregates or clusters within the silicate melt. In the case of laurite inclusions, such clusters must coalesce and react with available sulfur prior to entrapment in order to produce the observed micrometric inclusions of stoichiometric RuS_2.
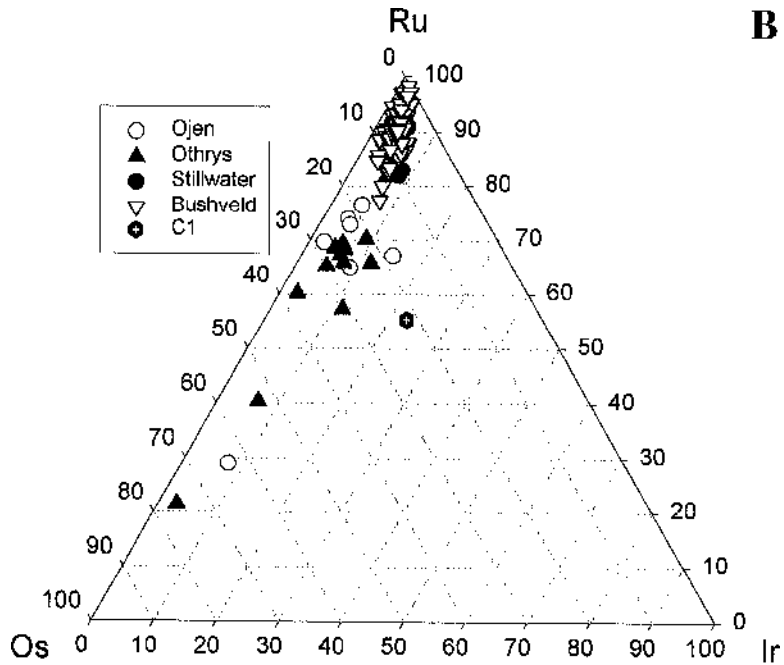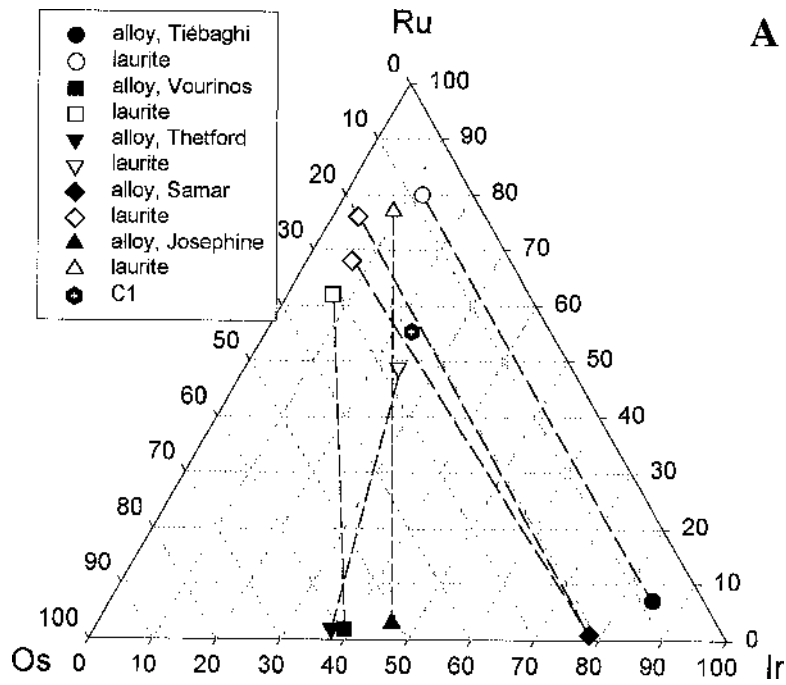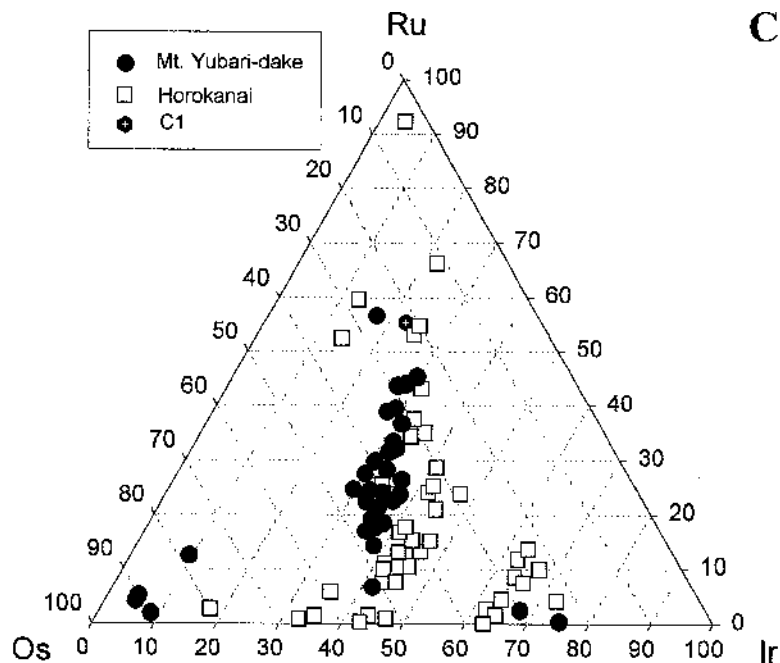
Fig. 11.   Triangular diagrams (atomic %) depicting representative compositions of A) laurite and associated Ru–Ir–Os alloy (all occurrences from ophiolite complexes), B) laurite as the sole primary IPGE mineral (occurrences from layered intrusions and ophiolites), and C) Ru–Os–Ir alloy as the sole primary IPGE mineral. Sources of data are: Tiébaghi ophiolite, New Caledonia (Augé 1988), Vourinos ophiolite, Greece (Augé 1985), Thetford ophiolite, Canada (Corrivaux & Laflamme 1990), Samar ophiolite, Philippines and Kamuikotan ophiolite, Japan (Nakagawa & Franco 1997), Josephine ophiolite, Oregon (Stockman & Hlava 1984), Bushveld intrusion, South Africa (Maier *et al.* 1999), Stillwater intrusion, Montana (Talkington & Lipin 1986), Ojen ophiolite, Spain (Torres-Ruiz *et al.* 1996), Othrys ophiolite, Greece (Garuti *et al.* 1999), C1 = C1 chondrite from Barnes *et al.* (1985).

Clearly, early precipitation and accumulation of laurite + Ru–Os–Ir alloy will have a profound effect on IPGE/PPGE fractionation, owing to the relative incompatibility of the PPGE in both of these PGM. Whether or not these phases begin to precipitate from a silicate magma will depend on the factors that control PGE solubility, which are as yet poorly constrained, but certainly include $f(O_2)$ (*e.g.,* O'Neill *et al.* 1995, Ertel *et al.* 1999, Amossé *et al.* 2000). An additional important question in determining the stability of laurite and Ru–Os–Ir alloy is whether the system reaches saturation in an immiscible sulfide liquid. We have found that 1 to >10 wt% Ru is required for laurite or alloy saturation in the sulfide liquid, and such levels are significantly higher than those expected for sulfide liquids produced by natural mafic magmas. Moreover, the high solubility of Ir alloy in molten sulfide (~4 wt%) documented by Peach & Mathez (1996) extends this result to Ir-rich composi-

tions. Such results virtually preclude the presence of laurite or Ru–Os–Ir alloy in magmatic systems that reach sulfide liquid saturation, as presaged by Merkle (1992), on the basis of textural observations of Bushveld chromitites. Thus, the presence of laurite or alloy (or both) as inclusions in primary chromian spinel in settings like the Bushveld or Stillwater complexes would suggest that initial crystallization took place under sulfide-liquid-undersaturated conditions. Early crystallization of laurite would be very effective in removing the IPGE from the magma, thus concentrating them in the initial cumulates, and resulting in a relative enrichment of the PPGE in the later-formed sulfide liquid. The abundances of PPGE would thereby be controlled by the fraction of sulfide liquid present in a particular rock-unit, and such relations have been well documented in the Bushveld (*i.e.,* Maier & Barnes 1999). For the case of sulfur-poor magmas, which never reach sulfide-liquid

saturation, precipitation of laurite or Ru–Os–Ir alloy (or both) will cause IPGE enrichment in the early-formed cumulates, with further crystallization causing progressive PPGE enrichment in the more evolved compositions. Peck & Keays (1990) have provided a detailed account of this behavior in the Heazlewood River Complex (Tasmania), which has an abundance of Ru–Os–Ir placer deposits derived from the basal cumulates, and no associated sulfide mineralization. This process also may act in the suboceanic upper mantle, as represented by ophiolite complexes, and may, in part, provide an explanation for the relative depletion of IPGE in mid-ocean-ridge basalts (Barnes *et al.* 1985). For magmas whose sulfur fugacities are sufficiently high that sulfide saturation occurs concurrently with the precipitation of the primary liquidus phases, laurite + Ru–Os–Ir alloy will not form, and decoupling of the IPGE from the PPGE can only occur by crystallization of *Mss* (*e.g.,* Li *et al.* 1998), as has been documented at Sudbury (Keays & Crockett 1970, Naldrett *et al.* 1982, Li *et al.* 1992), Noril'sk (Naldrett *et al.* 1994, Zientek *et al.* 1994) and Alexo, Ontario (Barnes & Naldrett 1986).

REFERENCES

AMOSSÉ, J., DABLE, P. & ALLIBERT, M. (2000): Thermochemical behaviour of Pt, Ir, Rh and Ru vs fO_2 and fS_2 in a basaltic melt. Implications for the differentiation and precipitation of these elements. *Mineral. Petrol.* **68**, 29-62.

AUGÉ, T. (1985): Platinum-group-mineral inclusions in ophiolitic chromitite from the Vourinos Complex, Greece. *Can. Mineral.* **23**, 163-171.

_____ (1988): Platinum-group minerals in the Tiebaghi and Vourinos ophiolitic complexes: genetic implications. *Can. Mineral.* **26**, 177-192.

BARIN, I. (1995): *Thermochemical Data of Pure Substances.* VCH Publishers, New York, N.Y.

BARNES, S.-J. & NALDRETT, A.J. (1986): Variations in platinum group element concentrations in the Alexo mine komatiite, Abitibi greenstone belt, northern Ontario. *Geol. Mag.* **123**, 515-524.

_____, _____ & GORTON, M.P. (1985): The origin of the fractionation of the platinum group elements in terrestrial magmas. *Chem. Geol.* **53**, 303-323.

_____, MAKOVICKY, E., MAKOVICKY, M., ROSE-HANSEN, J. & KARUP-MØLLER, S. (1997): Partition coefficients for Ni, Cu, Pd, Pt, Rh, and Ir between monosulphide solid solution and sulphide liquid and the formation of compositionally-zoned Ni–Cu sulphide bodies by fractional crystallization of sulphide liquid. *Can. J. Earth Sci.* **34**, 366-374.

_____ & PICARD, C.P. (1993): The behaviour of platinum-group elements during partial melting, crystal fractionation, and sulfide segregation: an example from the Cape Smith Fold Belt, northern Quebec. *Geochim. Cosmochim. Acta* **57**, 79-87.

BEZMEN, N.I., ASIF, M., BRÜGMANN, G.E., ROMANENKO, I.M. & NALDRETT, A.J. (1994): Distribution of Pd, Rh, Ru, Ir, Os, and Au between sulfide and silicate metals. *Geochim. Cosmochim. Acta* **58**, 1251-1260.

BRENAN, J.M. & CACIAGLI, N.C. (2000): Fe–Ni exchange between olivine and sulphide liquid: implications for oxygen barometry in sulphide-saturated magmas. *Geochim. Cosmochim. Acta* **64**, 307-320.

BRÜGMANN, G.E., ARNDT, N.T., HOFMANN, A.W. & TOBSCHALL, H.J. (1987): Noble metal abundances in komatiite suites from Alexo, Ontario and Gorgona Island, Colombia. *Geochim. Cosmochim. Acta* **51**, 2159-2169.

CAPOBIANCO, C.J. & DRAKE, M.J. (1990): Partitioning of ruthenium, rhodium and palladium between spinel and silicate melt. *Geochim. Cosmochim. Acta* **54**, 869-874.

_____, HERVIG, R.L. & DRAKE, M.J. (1994): Experiments on crystal/liquid partitioning of Ru, Rh and Pd for magnetite and hematite solid solutions crystallized from silicate melt. *Chem. Geol.* **113**, 23-43.

CARROLL, M.R. & WEBSTER, J.D. (1994): Solubilities of sulfur, noble gases, nitrogen, chlorine and fluorine in magmas. *In* Volatiles in Magmas (M.R. Carroll & J.R. Holloway, eds.). *Rev. Mineral.* **30**, 231-279.

CROCKET, J.H. (1981): Geochemistry of the platinum-group elements. *In* Platinum-Group Elements: Mineralogy, Geology, Recovery (L.J. Cabri, ed.). *Can. Inst. Mining Metall., Spec. Vol.* **24**, 47-64.

CORRIVAUX, L. & LAFLAMME, J.H.G. (1990): Minéralogie des éléments du groupe du platine dans les chromitites de l'ophiolite de Thetford Mines, Québec. *Can. Mineral.* **28**, 579-595.

ERTEL, W., O'NEILL, H. ST.C., SYLVESTER, P.J. & DINGWELL, D.B. (1999): Solubilities of Pt and Rh in a haplobasaltic silicate melt at 1300°C. *Geochim. Cosmochim. Acta* **63**, 2439-2449.

FLEET, M.E., CHRYSSOULIS, S.L., STONE, W.E. & WEISENER, C.G. (1993): Partitioning of platinum-group elements and Au in the Fe–Ni–Cu–S system: experiments on the fractional crystallization of sulfide melt. *Contrib. Mineral. Petrol.* **115**, 36-44.

_____, CROCKET, J.H. & STONE, W.E. (1996): Partitioning of platinum group elements (Os, Ir, Ru, Pt, Pd) and gold between sulfide liquid and basalt melt. *Geochim. Cosmochim. Acta* **60**, 2397-2412.

_____ & STONE, W.E. (1991): Partitioning of platinum-group elements in the Fe–Ni–S system and their fractionation in nature. *Geochim. Cosmochim. Acta* **55**, 245-253.

GARUTI, G., ZACCARINI, F. & ECONOMOU-ELIOPOULOS, M. (1999): Paragenesis and composition of laurite from chromitites of Othrys (Greece): implications for Os–Ru fractionation in ophiolitic upper mantle of the Balkan peninsula. *Mineral. Deposita* **34**, 312-319.

HARRIS, D.C. & CABRI, L.J. (1991): Nomenclature of platinum group element alloys: review and revision. *Can. Mineral.* **29**, 231-237.

HART, S.R. & RAVIZZA, G.E. (1996): Os partitioning between phases in lherzolite and basalt. *In* Earth Processes: Reading the Isotopic Code. *Am. Geophys. Union, Geophys. Monogr.* **95**, 123-134.

HAUGHTON, D.R., ROEDER, P.L. & SKINNER, B.J. (1974): Solubility of sulfur in mafic magmas. *Econ. Geol.* **69**, 451-467.

HIEMSTRA, S.A. (1979): The role of collectors in the formation of the platinum deposits in the Bushveld Complex. *Can. Mineral.* **17**, 469-482.

KEAYS, R.R. & CROCKET, J.H. (1970): A study of precious metal in the Sudbury nickel irruptive ores. *Econ. Geol.* **65**, 438-450.

KRESS, V. (1997): Thermochemistry of sulfide liquids. I. The system O–S–Fe at 1 bar. *Contrib. Mineral. Petrol.* **127**, 176-186.

LEGENDRE, O. & AUGÉ, T. (1986): Mineralogy of platinum-group mineral inclusions in chromitites from different ophiolite complexes. *In* Metallogeny of Basic and Ultrabasic Rocks (M.J. Gallagher, R.A. Ixer, C.R. Neary & H.M. Prichard, eds.). Institute of Mining Metallurgy, London, U.K. (361-375).

LI, CHUSI, BARNES, S.-J., MAKOVICKY, E., ROSE-HANSEN, J. & MAKOVICKY, M. (1998): Partitioning of nickel, copper, iridium, rhenium, platinum and palladium between monosulfide solid solution and sulfide liquid: effects of composition and temperature. *Geochim. Cosmochim. Acta* **60**, 1231-1238.

_____, NALDRETT, A.J., COATS, C.J.A. & JOHANNESSEN, P. (1992): Platinum, palladium, gold, and copper-rich stringers at the Strathcona mine, Sudbury: their enrichment by fractionation of a sulfide liquid. *Econ. Geol.* **87**, 1584-1598.

MAIER, W.D. & BARNES, S.-J. (1999): Platinum-group elements in silicate rocks of the lower, critical and main zones at Union Section, western Bushveld Complex. *J. Petrol.* **40**, 1647-1671.

_____, PRICHARD, H.M., FISHER, P.C. & BARNES, S.-J. (1999): Compositional variation of laurite at Union Section in the western Bushveld Complex. *S. Afr. J. Geol.* **102**, 286-292.

MERKLE, R.K.W. (1992): Platinum-group minerals in the middle group of chromitite layers at Marikana, western Bushveld Complex: indications for collection mechanisms and postmagmatic modification. *Can. J. Earth Sci.* **29**, 209-221.

NAKAGAWA, M. & FRANCO, H.E.A. (1997): Placer Os–Ir–Ru alloys and sulfides: indicators of sulfur fugacity in an ophiolite? *Can. Mineral.* **35**, 1441-1452.

NALDRETT, A.J., INNES, D.G., SOWA, J. & GORTON, M.P. (1982): Compositional variations within and between five Sudbury ore deposits. *Econ. Geol.* **77**, 1519-1534.

_____, PESSARAN, A., ASIF, M. & LI, CHUSI (1994): Compositional variation in the Sudbury ores and prediction of the proximity of footwall copper–PGE orebodies. *In* The Sudbury Noril'sk Symposium (P.C. Lightfoot & A.J. Naldrett, eds.). *Ont. Geol. Surv., Spec. Publ.* **5**, 133-143.

O'NEILL, H.ST.C., DINGWELL, D.B., BORISOV, A., SPETTEL, B. & PALME, H. (1995): Experimental petrochemistry of some highly siderophile elements at high temperatures, and some implications for core formation and the mantle's early history. *Chem. Geol.* **120**, 255-273.

PEACH, C.L. & MATHEZ, E.A. (1996): Constraints on the formation of platinum-group element deposits in igneous rocks. *Econ. Geol.* **91**, 439-450.

PECK, D.C. & KEAYS, R.R. (1990): Insights into the behavior of precious metals in primitive, S-undersaturated magmas: evidence from the Heazlewood River Complex, Tasmania. *Can. Mineral.* **28**, 553-557.

_____, _____ & FORD, R.J. (1992): Direct crystallisation of refractory platinum-group element alloys from boninitic magmas: evidence from western Tasmania. *Aust. J. Earth Sci.* **39**, 373-387.

PRICHARD, H.M., NEARY, C.R. & POTTS, P.J. (1986): Platinum group minerals in the Shetland ophiolite. *In* Metallogeny of Basic and Ultrabasic Rocks (M.J. Gallagher, R.A. Ixer, C.R. Neary & H.M. Prichard, eds.). Institute of Mining and Metallurgy, London, U.K. (395-414).

RICHARDSON, F.D. & FINCHAM, C.J.B. (1956): Sulphur in silicate and aluminate slags. *J. Iron Steel Inst.* **178**, 4-15.

ROEDER, P.L. & REYNOLDS, I. (1991): Crystallization of chromite and chromium solubility in basaltic melts. *J. Petrol.* **32**, 909-934.

SATTARI, P., BRENAN, J.M., MCDONOUGH, W.F. & HORN, I. (1999): Chromite–melt partitioning of Re and the PGEs. *Geol. Assoc. Can. – Mineral. Assoc. Can., Program Abstr.* **24**, 109.

STOCKMAN, H.W. & HLAVA, P.F. (1984): Platinum-group minerals in alpine chromitites from southwestern Oregon. *Econ. Geol.* **79**, 491-508.

STONE, W.E., CROCKET, J.H. & FLEET, M.E. (1990): Partitioning of palladium, iridium, platinum and gold between sulfide liquid and basalt melt at 1200°C. *Geochim. Cosmochim. Acta* **54**, 2341-2344.

TALKINGTON, R.W. & LIPIN, B.R. (1986): Platinum-group minerals in chromite seams of the Stillwater Complex, Montana. *Econ. Geol.* **81**, 1179-1186.

TORRES-RUIZ, J., GARUTI, G., GAZZOTTI, M., GERVILLA, F. & FENOLL HACH-ALÍ, P. (1996): Platinum-group minerals in chromitites from the Ojen lherzolite massif (Serrania de Ronda, Betic Cordillera, southern Spain). *Mineral. Petrol.* **56**, 25-50.

TREDOUX, M., LINDSAY, N.M., DAVIES, G. & MCDONALD, I. (1995): The fractionation of platinum-group elements in magmatic systems, with the suggestion of a novel causal mechanism. *S. Afr. J. Geol.* **98**, 157-167.

WALLACE, P. & CARMICHAEL, I.S.E. (1992): Sulfur in basaltic magmas. *Geochim. Cosmochim. Acta* **56**, 1863-1874.

ZIENTEK, M.L., LIKHACHEV, A. P., KUNILOV, V. E., BARNES, S.-J., MEIER, A.L., CARLSON, R..R., BRIGGS, P.H., FRIES, T.L. & ADRIAN, B.M. (1994): Cumulus processes and the composition of magmatic ore deposits: examples from the Talnakh district, Russia. *In* The Sudbury Noril'sk Symposium (P.C. Lightfoot & A.J. Naldrett, eds.). *Ont. Geol. Surv., Spec. Publ.* **5**, 133-146.